Subcortical Circuits Mediate Communication Between Primary Sensory Cortical Areas

Michael Lohse*[1], Johannes C. Dahmen[1], Victoria M. Bajo[1], Andrew J. King*[1]

[1]Department of Physiology, Anatomy, and Genetics. University of Oxford, Oxford OX1 3PT, United Kingdom.

*Correspondence should be addressed to M.L. (michael.lohse@dpag.ox.ac.uk) or A.J.K. (andrew.king@dpag.ox.ac.uk)

ACKNOWLEDGMENTS

The research was funded by a Wellcome Trust Studentship (WT105241/Z/14/Z) to M.L., and a Wellcome Trust Principal Research Fellowship (WT108369/Z/2015/Z) to A.J.K.

AUTHOR CONTRIBUTIONS

M.L. conceived and designed the research. M.L. performed research and analyzed the data. M.L. and J.C.D. performed surgeries. M.L. and A.J.K. acquired funding for the research. A.J.K. provided infrastructure and resources. A.J.K, J.C.D., and V.M.B. supervised the research. M.L., J.C.D., V.M.B. and A.J.K. interpreted the research. M.L., J.C.D., V.M.B. and A.J.K wrote the manuscript.

CONFLICT OF INTEREST

The authors declare no conflict of interest

Summary

Integration of information across the senses is critical for perception and is a common property of neurons in the cerebral cortex, where it is thought to arise primarily from corticocortical connections. Much less is known about the role of subcortical circuits in shaping the multisensory properties of cortical neurons. We show that stimulation of the whiskers causes widespread suppression of sound-evoked activity in mouse primary auditory cortex (A1). This suppression depends on the primary somatosensory cortex (S1), and is implemented through a descending circuit that links S1, via the auditory midbrain, with thalamic neurons that project to A1. Furthermore, a direct pathway from S1 has a facilitatory effect on auditory responses in higher-order thalamic nuclei that project to other brain areas. Crossmodal corticofugal projections to the auditory midbrain and thalamus therefore play a pivotal role in integrating multisensory signals and in enabling communication between different sensory cortical areas.

Introduction

Having multiple sensory systems, each specialized for the transduction of a different type of physical stimulus, maximizes our ability to gather information about the external world. Furthermore, when the same event or object is registered by more than one sense, as is often the case, our chances of detecting and accurately evaluating its biological significance dramatically increase (Murray and Wallace, 2012). Unlike audition and vision, the sense of touch informs an organism exclusively about objects in its immediate vicinity. This is particularly important in animals that rely on their whiskers for detecting the presence and location of objects as they explore their surroundings (Diamond et al., 2008). Inputs from the whiskers can enhance sound-induced defensive behavior (Wang et al., 2019) and neural mechanisms that give precedence to the processing of somatosensory information over cues from other modalities are likely to be advantageous to the organism's survival.

Apart from specialized subcortical premotor nuclei, such as the superior colliculus, it is widely assumed that multisensory processing is most prevalent at the level of the cerebral cortex (Choi et al., 2018; Murray and Wallace, 2012). Evidence for multisensory convergence has been found in nearly all cortical areas, including the primary sensory cortices. In the primary auditory cortex (A1), for example, visual or tactile stimuli can modulate acoustically-driven activity, most commonly by suppressing responses to sound in both awake and anesthetized animals (Bizley et al., 2007; Kayser et al., 2008; Meredith and Allman, 2015; Rao et al., 2014). Suppression of sound-evoked activity in auditory cortical neurons by somatosensory inputs likely provides a mechanism for prioritizing the processing of tactile cues from nearby objects that require urgent attention.

The circuitry underlying crossmodal influences on processing in early sensory cortical areas is poorly understood. Because visual, auditory and somatosensory cortices innervate each other and receive inputs from higher-level, association areas (Banks et al., 2011; Bizley et al., 2007; Budinger et al., 2006; Cappe and Barone, 2005; Meredith and Allman, 2015; Rockland and Ojima, 2003; Stehberg et al., 2014; Zingg et al., 2014), most studies have focused on the role of intracortical circuits in multisensory integration (Atilgan et al., 2018; Ibrahim et al., 2016; Iurilli et al., 2012; Song et al., 2017). This, however, ignores the potential contribution of ascending inputs from the thalamus, which may also provide a source of multisensory input to primary cortical areas, such as A1 (Budinger et al., 2006; Chou et al., 2020; Khorevin, 1980; Kimura and Imbe, 2018; Wu et al., 2015), or the possibility that early sensory cortical areas may communicate via a combination of corticofugal and thalamocortical pathways (Lohse et al., 2019; Sherman and Guillery, 2011).

We show that somatosensory inputs exert a powerful influence on processing in the auditory system, which takes the form of divisive suppression in the auditory thalamus and cortex. Dissecting

the underlying circuitry, we found that this suppression originates in the primary somatosensory cortex (S1) and is implemented via S1-recipient neurons in the auditory midbrain, which inhibit sound-driven activity in the auditory thalamocortical system. We also show that a parallel crossmodal corticothalamic pathway from S1 to the medial sector of the auditory thalamus allows for somatosensory facilitation of auditory responses in thalamic neurons that do not project to the auditory cortex. These results demonstrate that the auditory midbrain and thalamus have essential roles in integrating somatosensory and auditory inputs and in mediating communication between cortical areas that belong to different sensory modalities.

Results

Somatosensory influences on primary auditory cortex

Because variable effects of tactile stimulation have been reported on the activity of neurons in the auditory cortex of different species (Fu et al., 2003; Kayser et al., 2005; Meredith and Allman, 2015; Rao et al., 2014; Zhang et al., 2020), we recorded extracellular activity in A1, identified by its tonotopic gradient, while presenting sounds to mice and simultaneously deflecting their whiskers (Figure 1A). We consistently found that concurrent whisker stimulation reduced auditory responses evoked by both tones (Figure 1B-D) and noise bursts (Figure 1E,F), demonstrating widespread suppression of auditory activity in A1. These findings in anesthetized mice are in accordance with reports of pronounced inhibition of A1 activity by facial touch in freely-moving rodents (Rao et al., 2014), therefore indicating that the suppression of auditory responses by whisker stimulation is unlikely to be due to changes in attention, locomotion or arousal. Furthermore, assessment of the input-output responses across all tones presented, normalized to the firing rate at each neuron's best frequency (BF), revealed that this suppression was stimulus specific and of a divisive nature, with strong effects around the BF and negligible effects for off-BF responses that were closer to baseline activity (Figure 1D).

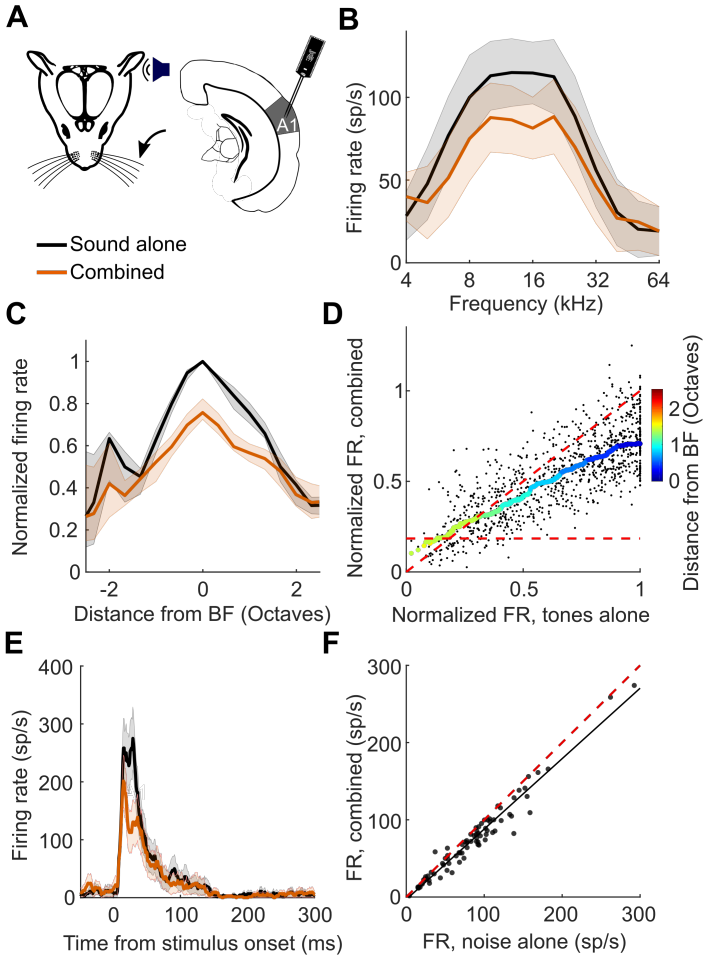

Figure 1. Somatosensory suppression of neurons in primary auditory cortex.

(A) Schematic of recording setup. (B) Frequency tuning curves with (orange) and without (black) whisker deflection from an example unit in A1. (C) Median frequency tuning across all tuned A1 units with and without whisker deflection (change in BF response: $P < 0.001$, $n = 77$, 4 mice). (D) Relationship between normalized firing rate (FR) to tones across all frequencies and all units (black dots) with ('combined') or without ('tones alone') whisker stimulation. Thick multi-colored line denotes the running median of this relationship (window: 0.1 normalized firing rate), and the colors denote distance from BF. The horizontal dashed red line denotes the median normalized spontaneous rate across units. The diagonal dashed red line is the line of equality. A larger distance between the multi-colored line and the diagonal line at the blue end than at the red end indicates divisive scaling. (E) An A1 example unit's responses to broadband noise with (orange) and without (black) concurrent whisker stimulation. (F) Summary of A1 units' responses to noise alone vs noise with whisker deflection ($P < 0.001$, $n = 81$, 4 mice). FR, firing rate. The red dashed line indicates the line of equality. The black solid line indicates the least squares linear fit. Shaded area indicates 95% confidence intervals of the mean (B,E) or 95% nonparametric confidence intervals of the median (C).

Somatosensory influences on auditory thalamus

To investigate the circuitry underlying this extensive modulation of auditory cortical processing, we first set out to determine whether the activity of subcortical auditory neurons is similarly affected by whisker stimulation. We found no evidence for somatosensory-auditory interactions in the central

nucleus of the inferior colliculus (CNIC) (Figure S1) and therefore focused on the medial geniculate body (MGB), the main thalamic gateway to the auditory cortex. We recorded from neurons in the lateral region of the MGB, including both the lemniscal ventral division (MGBv) and the non-lemniscal dorsal division (MGBd) (Figure 2 and Figure S2). Whisker stimulation suppressed responses to noise and to tones near the BF of neurons in both MGBv and MGBd (Figure 2B-D and Figure S3). As in the cortex, this suppression took the form of a divisive scaling of the sound-evoked response (Figure 2E,F). Whisker stimulation alone did not affect the activity of neurons in either MGBv or MGBd (Figure S3).

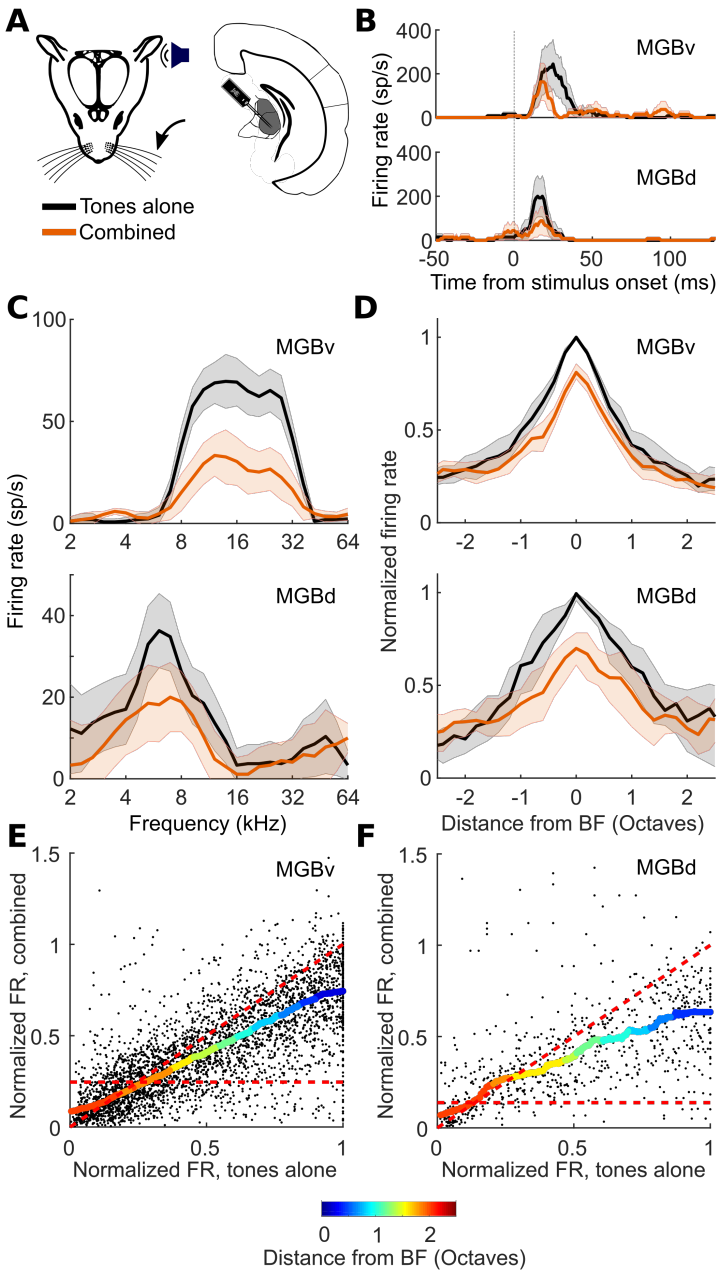

Figure 2. Divisive scaling of frequency tuning in the MGBv and MGBd

(A) Schematic of recording setup. (B) Examples of PSTHs illustrating BF responses with (orange) or without (black) concurrent whisker stimulation from units in MGBv and MGBd. (C) Examples of frequency tuning curves with or

without concurrent whisker stimulation from units in MGBv and MGBd. (D) Median tuning curve across units recorded in MGBv (change in BF response: $P < 0.001$, $n = 145$) or MGBd (change in BF response, $P < 0.001$, $n = 31$) with or without concurrent whisker stimulation. Shaded area indicates the 95% confidence intervals of the means (B,C), or the 95% nonparametric confidence intervals of the median (D). (E,F) Relationship between normalized firing rate (FR) for all units (black dots) recorded in the MGBv (E) and MGBd (F) in response to tones across all frequencies presented either with ('combined') or without ('tones alone') whisker stimulation. Thick multi-colored lines show the running median of this relationship (window: 0.1 normalized firing rate), and the colors denote distance from BF. The horizontal dashed red line denotes the median normalized spontaneous rate across units. The diagonal dashed red line is the line of equality. A larger distance between the multi-colored line and the diagonal line at the blue end than at the red end indicates divisive scaling. $n_{MGBv} = 145$ (9 mice); $n_{MGBd} = 31$ (9 mice).

The medial section of the auditory thalamus contains several divisions, medial MGB (MGBm), the posterior intralaminar nucleus (PIN), and the suprageniculate nucleus (SGN), which are anatomically distinct from the MGBv and MGBd (Anderson and Linden, 2011; Lu et al., 2009; Vasquez-Lopez et al., 2017). In the MGBm/PIN and SGN, we found units that were directly driven by whisker inputs alone (Figure 3A,C,I). We also found that the responses of individual units to noise (Figure 3A,B,D,I) or tones (Figure 3I) could be either facilitated or suppressed when combined with whisker input. Units in which responses to tones were facilitated exhibited an increase in firing rate across the entire frequency tuning curve, indicative of additive scaling (Figure 3E,F), whereas suppressed units, similar to those in MGBv/d and cortex, showed divisive scaling (Figure 3G,H). Thus, neurons in the medial section of the auditory thalamus were influenced by whisker stimulation in a much more heterogeneous fashion than neurons in the lateral MGB (Figure 3J).

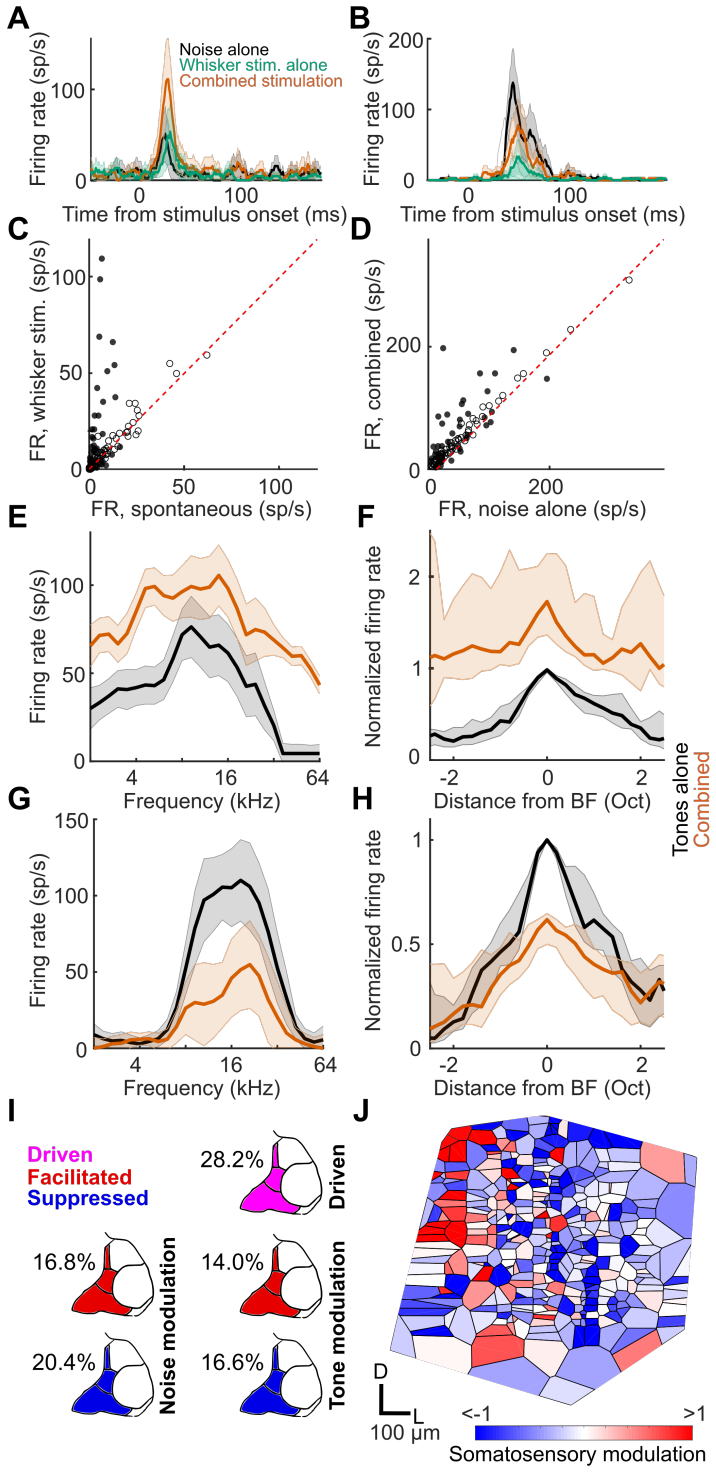

Figure 3. Diverse somatosensory influences on neurons in MGBm/PIN and SGN

(A,B) Example PSTHs of responses to broadband noise recorded in MGBm/PIN/SGN with (orange) and without (black) concurrent whisker stimulation, as well as whisker stimulation alone (green) showing facilitation (A, $P < 0.05$, paired *t*-test) and suppression (B, $P < 0.05$, paired *t*-test) of the auditory response, respectively. (C) Summary of responses (firing rate, FR) to whisker stimulation alone vs spontaneous activity in the medial sector of the auditory thalamus. Filled circles indicate units driven by somatosensory stimulation ($P < 0.05$, *t*-test). (D) Summary of responses to broadband noise combined with or without concurrent whisker stimulation. Filled circles indicate significantly ($P < 0.05$, paired *t*-test) modulated units (n = 113, 8 mice). (E) Example frequency

tuning curves for tones with (orange) and without (black) concurrent whisker stimulation for a unit showing crossmodal facilitation ($P < 0.05$, paired *t*-test). (F) Summary tuning curves of units with significantly facilitated BF responses. (G,H) Same as E-F for units with significantly suppressed BF responses. $n_{facilitated} = 32$, $n_{suppressed} = 27$, 12 mice. Shaded area indicates 95% confidence intervals of the mean (A,B,E,G) or nonparametric confidence intervals of the medians (F,H), respectively. (I) Percentage of neurons in the MGBm/PIN and SGN significantly ($P < 0.05$, one-sided *t*-test) driven by somatosensory input, or showing significant modulation ($P < 0.05$, two sided *t*-test) of the responses to noise or tones at BF when combined with somatosensory input. (J) Voronoi diagram illustrating somatosensory modulation in all tuned neurons across auditory thalamus. Each patch represents the location of one extracellularly recorded thalamic unit (n = 369, 14 mice) and is color-coded for the type and strength of somatosensory modulation (red, facilitation; blue, suppression).

Somatosensory inhibition of auditory cortex is inherited from the thalamus

Whisker-stimulation induced suppression of auditory activity is therefore present subcortically, particularly in the MGBv and MGBd, two auditory thalamic subdivisions with massive thalamocortical projections. This suggests that cortical neurons may inherit signals in which acoustic and somatosensory information have already been integrated. To investigate whether MGB neurons do indeed relay a whisker-modulated signal to auditory cortex, we expressed the calcium indicator GCaMP6m in the entire auditory thalamus and measured calcium transients in thalamocortical boutons in layer 1 of the auditory cortex (Vasquez-Lopez et al., 2017) (Figure 4A,B). Layer 1 of the mouse auditory cortex tends to receive more diverse thalamic inputs than layers 3b/4. In A1, for example, layer 1 combines dense projections from MGBv (Takesian et al., 2018; Vasquez-Lopez et al., 2017) with projections from other structures, such as MGBm (Vasquez-Lopez et al., 2017) and the lateral posterior nucleus of the thalamus (Chou et al., 2020). Nevertheless, whisker stimulation had a suppressive effect on responses to both noise (Figure 4C,D) and tones (Figure 4E,F). Similar to neurons in MGBv, MGBd and auditory cortex, frequency-tuned thalamocortical boutons exhibited divisive scaling with the largest response reduction at BF (Figure 4E,F). We did not find any auditory thalamocortical boutons that were driven by whisker stimulation alone or whose sound responses were facilitated by whisker stimulation. This suggests that only somatosensory suppression of auditory activity is projected to the auditory cortex, whereas the facilitation observed in the medial sector of the auditory thalamus is not.

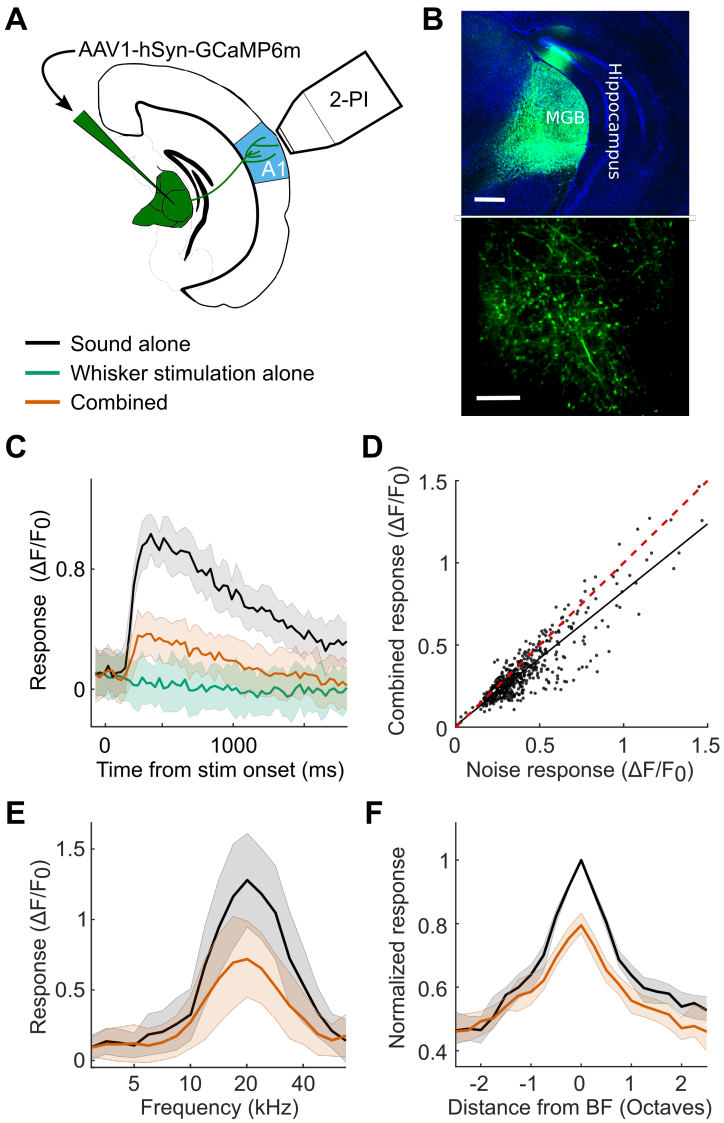

Figure 4: Thalamic inputs to auditory cortex are suppressed by whisker stimulation

(A) Schematic of recording setup. (B) *Top:* Confocal image of GCaMP6m expression in the auditory thalamus. Scale bar, 400 µm. *Bottom: In vivo* 2-photon image of thalamocortical boutons in layer 1 of the auditory cortex. Scale bar, 20 µm. (C) Calcium response of an example thalamic bouton in layer 1 responding to broadband noise with (orange) or without (black) concurrent whisker deflection, as well as to whisker deflection alone (green). (D) Summary of responses to noise alone vs combined noise plus whisker deflection in all noise-responsive thalamocortical boutons ($P < 0.001$, $n = 512$, 3 mice). The red dashed line indicates the line of equality. The black solid line indicates the least squares linear fit. (E) Frequency tuning curves with (orange) and without (black) whisker deflection from an example thalamocortical bouton. (F) Median frequency tuning curves across all frequency tuned boutons (change in BF response: $P < 0.001$, $n = 310$, 3 mice). Shaded area indicates the 95% confidence intervals of the means (C,E), or the 95% nonparametric confidence intervals of the median (F).

S1 mediates suppression of the auditory thalamus

To determine whether the primary somatosensory cortex (S1) is involved in whisker-stimulation induced suppression of the auditory thalamocortical system, we recorded neuronal activity in the MGB of VGAT-ChR2-YFP mice whilst silencing S1 optogenetically (Figure 5A and Figure S4). Silencing S1 did not affect spontaneous activity or tone-evoked auditory thalamic responses (Figure S4), but significantly reduced the capacity of whisker stimulation to suppress the BF responses of neurons in both MGBv and MGBd (Figure 5B,C). Thus, S1 is a critical part of the circuitry mediating the somatosensory control of auditory thalamocortical responses.

Silencing S1 also had a similar effect on the responses of neurons in the medial sector of the auditory thalamus that were otherwise robustly suppressed by whisker stimulation (Figure S5), but did not affect the capacity of whisker stimulation to enhance responses in this part of the thalamus (Figure S5). S1 is thus necessary for somatosensory suppression throughout the auditory thalamus, but not for somatosensory facilitation. That S1 activation is also sufficient for the suppression of auditory thalamocortical responses was revealed when we optogenetically activated infragranular cells in S1 via the red-shifted opsin ChrimsonR and measured calcium transients in thalamocortical boutons (Figure 5D,E). Optogenetic S1 activation suppressed their responses to noise bursts (Figure 5F,G) and thus replicated the previously observed whisker-induced suppression of auditory thalamocortical boutons.

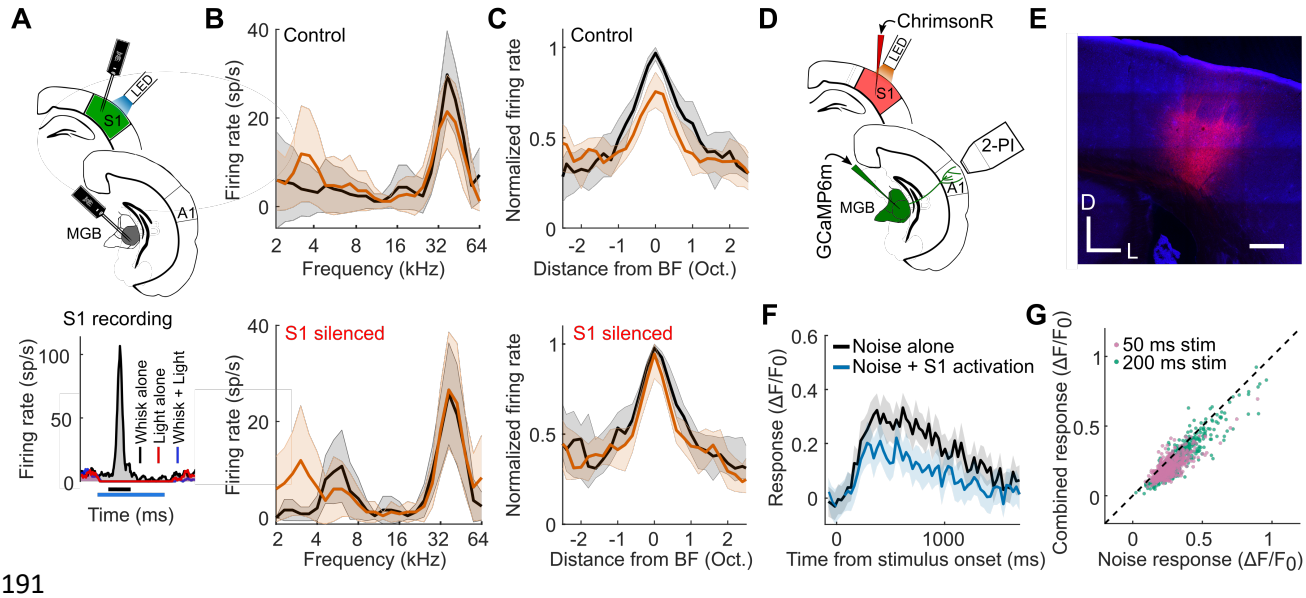

Figure 5: S1 mediates somatosensory suppression of auditory thalamocortical axons

(A) *Top:* Schematic of optogenetic targeting of somatosensory cortex in VGAT-ChR2 mice and electrophysiological recording setup. *Bottom:* Example PSTHs of a unit recorded in S1, demonstrating the effect of optogenetic suppression of somatosensory cortex on spontaneous activity and whisker-stimulation evoked

responses. Bars below the x-axis indicate timing of whisker stimulation (black) and light stimulation for silencing S1 (blue). (B) Frequency tuning curves of an example MGBv unit based on tone responses with (orange) and without (black) concurrent whisker stimulation during the control condition (top) and when S1 was silenced (bottom). (C) Median tuning curves of all units recorded in MGBv/d with (orange) and without whisker deflection (black) during the control condition (top) and when S1 was silenced (bottom). The suppressive effect of whisker stimulation on the BF response of MGBv/d neurons was reduced following S1 silencing ($P = 0.014$, $n = 59$, 3 mice). (D) Schematic of experimental setup for combined 2-photon thalamocortical bouton imaging with optogenetic activation of S1. (E) Confocal image showing expression of ChrimsonR-tdTomato in infragranular layers of S1. Scale bar, 300 µm. (F) Calcium response of an example thalamic bouton in layer 1 of the auditory cortex, illustrating suppression of the response to a 50 ms noise burst by optogenetic S1 stimulation. Shading indicates 95% confidence intervals around the mean. The 3rd and 4th imaging frames of the S1 stimulation condition displayed a large light artefact from the LED and have therefore been removed. (G) Summary plot of responses to noise alone or noise combined with infragranular S1 stimulation for all noise-responsive boutons. Purple and green points indicate responses to 50 ms and 200 ms noise stimulation, respectively. $n_{50ms} = 539$, 8 imaging fields, 1 mouse; $n_{200ms} = 652$, 7 imaging fields, 2 mice. Shaded area indicates the 95% confidence intervals of the means (B,F), or the 95% nonparametric confidence intervals of the median (C).

Auditory cortex does not mediate somatosensory influences on auditory thalamus

One way in which S1 could suppress neuronal activity in the auditory thalamus is via an indirect corticocorticothalamic route that takes advantage of the massive corticothalamic projections originating in the auditory cortex. However, while silencing auditory cortex strongly decreased both spontaneous activity (Figure S4) and sound-evoked responses in MGBv and MGBd neurons (Figure S4), we observed no change in either the response suppression evoked in these neurons by whisker stimulation (Figure S6) or in the response facilitation exhibited by neurons located in the medial sector of the auditory thalamus (Figure S6).

S1 projection neurons account for auditory thalamic facilitation

To investigate whether a direct corticothalamic projection (Allen et al., 2017; Lohse et al., 2019; Mo and Sherman, 2018) exists that could mediate somatosensory control over auditory thalamus, we performed viral tracing experiments in S1 corticothalamic neurons. These revealed that a projection does indeed exist, which originates from RBP4-expressing layer 5 neurons in S1 and densely innervates the medial sector of auditory thalamus (Figure 6A-C), particularly the PIN (Figure 6B,C). Optical stimulation of these S1 layer 5 neurons significantly altered the spontaneous firing rate of more than a third of recorded units (Figure 6D,E), suggesting a direct excitatory pathway from S1 to the medial auditory thalamus. Activation of this pathway also replicated the additive scaling of the frequency response profiles of auditory neurons recorded in this region of the auditory thalamus (Figure 6F,G) that we observed when combining sounds and whisker stimulation.

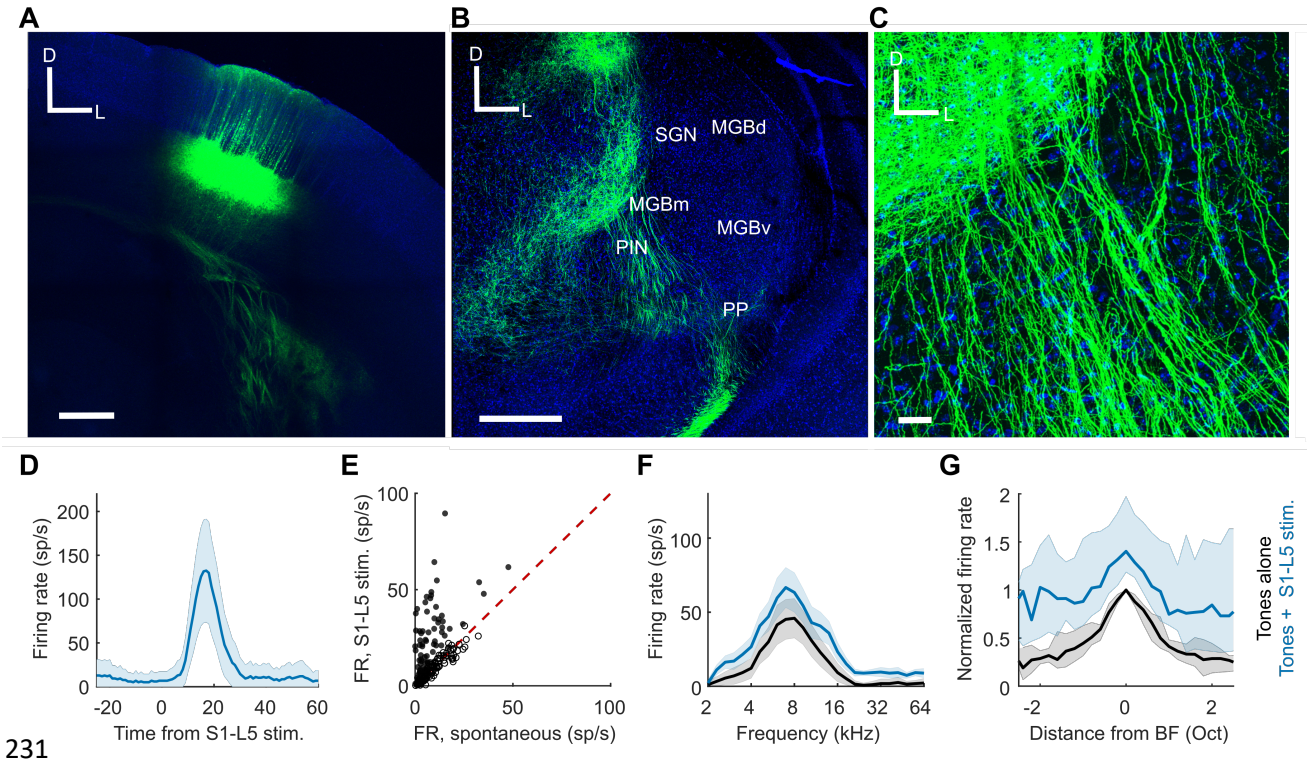

Figure 6: Direct pathway from S1 to MGBm/PIN and SGN

(A) Confocal image of ChR2-YFP expression in RBP4+ cells in layer 5 (L5) of S1. Scale bar, 400 µm; D, dorsal; L, lateral. (B) Confocal image of a coronal section of the thalamus showing S1-L5 (RBP4+) axons in the medial sector of the auditory thalamus. PP, peripeduncular nucleus. Scale bar, 400 µm. (C) High magnification image showing S1-L5 (RBP4+) axons in MGBm/PIN. Blue = DAPI, Green = YFP. Scale bar, 30 µm. (D) Example unit located in MGBm/PIN that was driven by stimulation of S1-L5 (RBP4+) neurons. (E) Summary of MGBm/PIN neuronal firing rate (FR) responses to 50 ms light pulses delivered to stimulate S1-L5 (RBP4+) neurons. *n* = 183, 5 mice. Filled circles indicate the 69 units in which spontaneous firing was significantly altered ($p < 0.05$, *t*-test) by S1-L5 stimulation. (F) Tuning curves from an example unit in MGBm/PIN in which the auditory response was significantly enhanced by concurrent stimulation of S1-L5 (RBP4+) neurons. (G) Median tuning curves from units in the medial sector of auditory thalamus with significantly ($p < 0.05$, paired *t*-test) facilitated BF responses during stimulation of S1-L5 (RBP4+) neurons. *n* = 25, 5 mice. Shaded areas indicate 95% confidence intervals of the means (D,F) or 95% nonparametric confidence intervals of the medians (G), respectively. BF responses were significantly modulated in 18% (13.7% facilitated, 4.4% suppressed; n= 183, 5 mice) of units in MGBm/PIN and SGN by concurrent stimulation of S1-L5 (RBP4+) neurons.

Although these findings are consistent with a facilitatory influence of layer 5 projection neurons in S1 on neurons in the medial auditory thalamus, selective stimulation of the RBP4-expressing neurons did not induce suppression of the sound-evoked responses of neurons recorded in the MGBv and MGBd (Figure S7). This result can be readily accounted for given the generally

excitatory nature of corticofugal projections and the predominantly medial termination pattern of this particular pathway, as well as the relative paucity of GABAergic interneurons in the rodent MGB (Winer and Larue, 1996). Nevertheless, the lack of effect from stimulation of S1 RBP4-expressing neurons on the sound-evoked responses of neurons recorded in the lateral auditory thalamus contrasts with the reduced influence of whisker stimulation on those responses when S1 was silenced optogenetically. This therefore implies the existence of another pathway by which S1 neurons can influence auditory processing in this part of the thalamus.

A corticocollicular pathway for somatosensory thalamic suppression

The final objective was to identify the source of inhibition mediating S1-dependent suppression of neuronal activity in the auditory thalamus. One major source of inhibitory input to the MGB, and a structure that has previously been implicated in crossmodal thalamic processing (Kimura et al., 2012), is the thalamic reticular nucleus (TRN). By optogenetically silencing the auditory sector of TRN (AudTRN) during tone presentation, we found that this part of the thalamus can modulate the excitability of MGB neurons (Figure 7A-C). Surprisingly, however, we did not find any evidence that AudTRN neurons play a role in mediating somatosensory suppression of the MGB (Figure 7D,E).

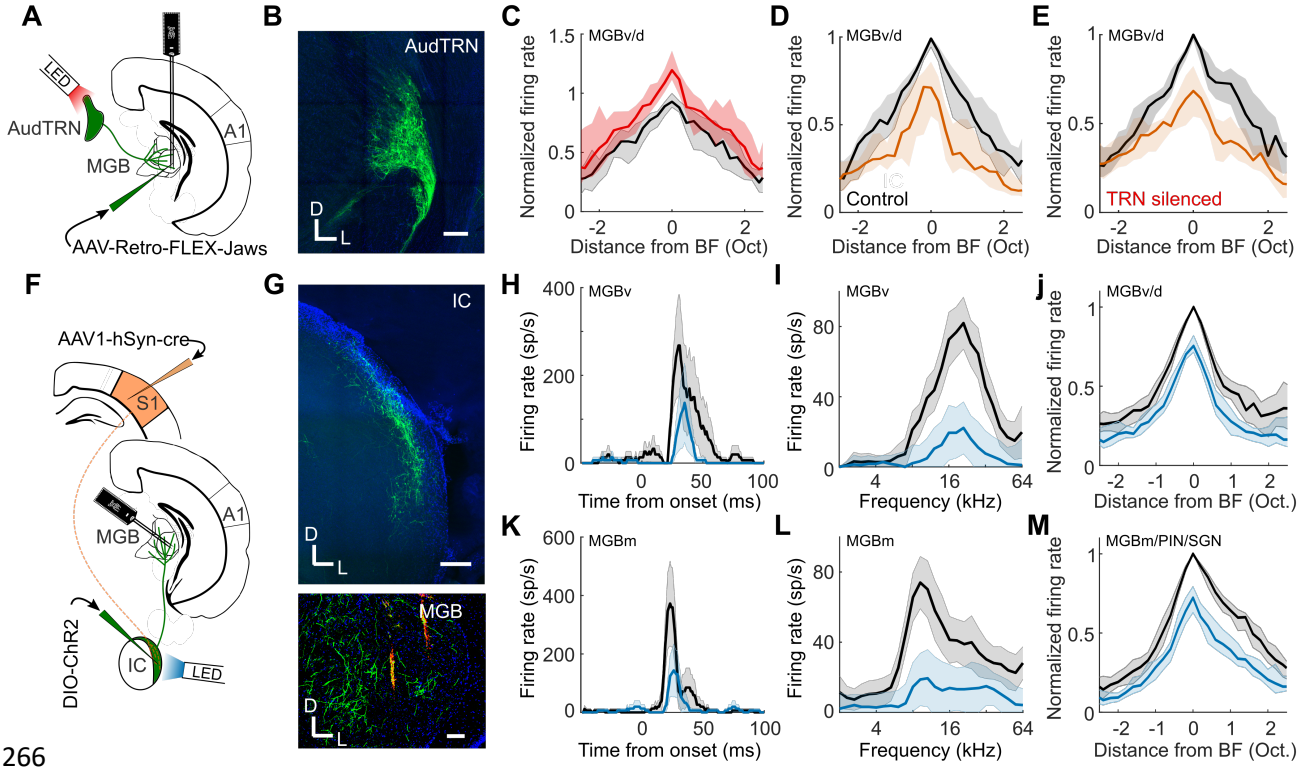

Figure 7: Corticocollicular circuit mediates somatosensory suppression of the thalamus

(A) Schematic of experimental paradigm in B-E. (B) GABAergic cells in TRN retrogradely-labelled with Jaws from auditory thalamus. Scale bar, 150 µm. (C) Summary (median) frequency tuning curve across MGBv/d units with (red) or without (black) optogenetic suppression of AudTRN activity (change in BF firing response, $P < 0.001$, n =

38, 2 mice). (D-E) Median frequency tuning curve of MGBv/MGBd units illustrating suppression induced by concurrent whisker stimulation (orange) with AudTRN either unaffected (D) or optogenetically suppressed (E). Silencing AudTRN had no effect on the whisker-induced suppression of auditory responses in MGBv/MGBd ($P = 0.83$, $n = 38$, 2 mice). (F) Schematic of experimental paradigm in G-M. (G) *Top:* ChR2-YFP expression in neurons in the shell of IC, labelled by anterograde transport of cre from S1 (AAV1-hSyn-cre) and a cre-dependent AAV5-DIO-ChR2-eYFP injected into the IC. Scale bar, 200 µm. *Bottom:* Axons (green) of anterogradely labelled IC neurons in MGB. Scale bar, 100 µm. Orange marks show DiI tracts from the recording probe in the MGB. D, dorsal; L, lateral. (H) Example PSTHs illustrating BF responses of an MGBv unit with (blue) and without (black) optogenetic stimulation of S1-recipient IC neurons. (I) Example frequency tuning curve of an MGBv unit with (blue) and without (black) optogenetic stimulation of S1-recipient IC neurons. (J) Median MGBv/MGBd tuning curve with (blue) and without (black) stimulation of S1-recipient IC neurons: -20.9% median change in BF firing rate ($P < 0.001$; $n = 85$, 3 mice). (K-M) same as H-J for units recorded in MGBm/PIN/SGN. (M) -26.9% median change in BF firing rate ($P < 0.001$; $n = 89$, 3 mice). Shaded area illustrates the 95% confidence intervals of the means (H,I,K,L), or the 95% nonparametric confidence intervals of the median (C,D,E,J,M).

Inhibitory input to the MGB can also arrive from extra-thalamic sources, including the IC (Beebe et al., 2018; Clarke and Lee, 2018; Lesicko et al., 2016), which provides its major source of ascending input. Interestingly, descending inputs from the somatosensory cortex appear to target modular zones containing GABAergic neurons within the lateral shell of the mouse IC (Lesicko et al., 2016), suggesting a possible route by which whisker stimulation could influence auditory processing. In order to selectively target IC neurons that receive input from S1, we employed an anterograde transsynaptic viral tagging approach (Zingg et al., 2017), which involved injecting AAV1-hSyn-cre into S1. Combining this with an injection into the IC of a virus that cre-dependently expresses both channelrhodopsin-2 and eYFP, we were able to show that S1 targets a subset of IC shell neurons (Figure 7F,G) and that these neurons project to the auditory thalamus (Figure 7G). Furthermore, activating these S1-recipient IC neurons induced suppression of auditory responses both in MGBv/d (Figure 7H-J) and the medial auditory thalamus (Figure 7K-M). This demonstrates that S1 exerts suppressive control over auditory thalamic processing via a corticocolliculothalamic pathway, in addition to its facilitatory influence via a direct crossmodal corticothalamic pathway (Figure 8).

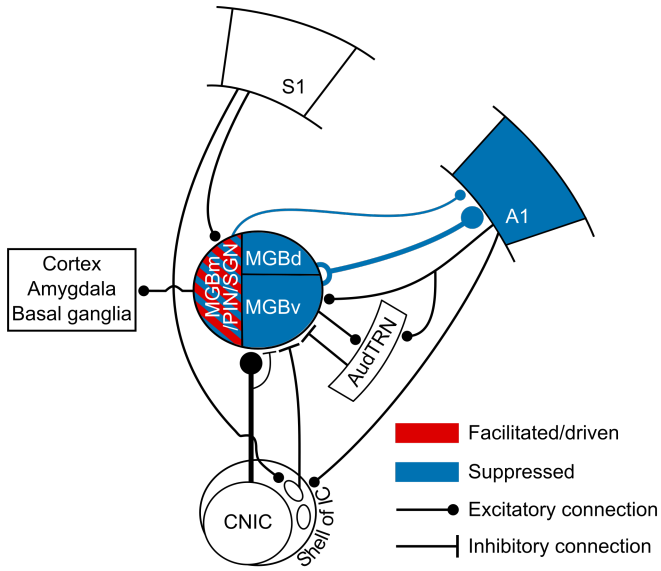

Figure 8: Circuits enabling somatosensory control of the auditory thalamocortical system.

Auditory responses in the regions of the auditory thalamus and cortex depicted in blue were suppressed by concurrent whisker stimulation via a descending pathway from S1 to the lateral shell of IC, which then projects to the MGB. Some neurons in the medial sector of the auditory thalamus were driven or had their auditory responses enhanced by whisker stimulation (depicted in red), which can be mediated by a direct corticothalamic projection from S1 to MGBm/PIN/SGN.

Discussion

Our results demonstrate that the somatosensory system exerts a powerful influence over sound processing in both the auditory cortex and thalamus. These effects are diverse and anatomically specific. We identified two separate corticofugal pathways (Figure 8), which both originate in S1 but exert opposing somatosensory control over the auditory thalamus. First, a crossmodal descending pathway via the auditory midbrain mediates somatosensory divisive suppression in the auditory thalamocortical system. Second, a direct corticothalamic pathway targets the medial sector of auditory thalamus, through which S1 drives spiking activity and facilitates neuronal responses that are not transmitted to the auditory cortex. These findings therefore reveal an unexpected role for corticofugal projections to both the auditory midbrain and thalamus in shaping the multisensory properties of auditory cortical and other downstream neurons and in enabling communication between different cortical areas.

Auditory cortex inherits multisensory signals from the thalamus

Multisensory interactions occur throughout the cerebral cortex, including early sensory areas (Choi et al., 2018; Murray and Wallace, 2012). Although spiking responses to visual or somatosensory stimuli have been found in different parts of auditory cortex, the commonest type of crossmodal interaction is seen in studies that paired otherwise ineffective stimuli with a sound (Atilgan et al., 2018; Bizley et al., 2007; Fu et al., 2003; Ghazanfar et al., 2005; Kayser et al., 2005, 2008; Lakatos et al., 2007; Meredith and Allman, 2015; Rao et al., 2014). Diverse modulatory effects on auditory cortical processing have been reported in these studies, and, in line with our results, several have found that crossmodal suppressive interactions are particularly prevalent, both in rodents (Chou et al., 2020; Rao et al., 2014; Zhang et al., 2020) and other species (Bizley et al., 2007; Kayser et al., 2008; Meredith and Allman, 2015; Perrodin et al., 2015).

The search for the source of these non-auditory influences on auditory cortical activity has focused principally on other cortical areas. Direct connections between early sensory cortical areas have been widely reported in different species (Banks et al., 2011; Bizley et al., 2007; Budinger et al., 2006; Cappe and Barone, 2005; Meredith and Allman, 2015; Rockland and Ojima, 2003; Stehberg et al., 2014). Furthermore, in mice, optogenetic stimulation of A1 corticocortical projections can modulate the activity (Ibrahim et al., 2016; Iurilli et al., 2012) and stimulus selectivity (Ibrahim et al., 2016) of neurons in primary visual cortex via local inhibitory circuits. These studies therefore highlight the importance of intracortical connections in mediating multisensory interactions.

Non-auditory influences on auditory cortical processing can also be inherited from the thalamus. Anatomical studies have emphasized the potential contribution to multisensory processing in the auditory cortex of extralemniscal thalamic input, not just from non-primary regions of the MGB, such as the MGBm, but also from areas like the SGN and the pulvinar (Budinger et al., 2006; De La Mothe et al., 2006; Smiley and Falchier, 2009). Indeed, in mice, the suppressive effects of visual looming stimuli on A1 activity appear to be mediated by the lateral posterior nucleus, the rodent homologue of the primate pulvinar (Chou et al., 2020). However, A1 receives the great majority of its ascending input from the MGBv, which is traditionally viewed as a unisensory structure. Nevertheless, cutaneous electrical stimulation has been shown to modulate auditory responses in the MGBv (Khorevin, 1980; Kimura and Imbe, 2018), and our findings demonstrate that the sound-evoked responses of most neurons recorded there and in the MGBd are suppressed by concurrent whisker stimulation. Moreover, we observed comparable crossmodal suppression in auditory thalamocortical axon boutons and in A1 neurons, indicating that somatosensory-auditory interactions are likely inherited by these cortical neurons from their primary source of thalamic input.

In the MGBv and MGBd, the strongest suppressive effects induced by whisker stimulation occurred at the BF of the neurons, i.e. the tone frequency at which the largest response was obtained. This crossmodal divisive scaling by non-driving sensory inputs resembles that found in primate cortex (Avillac et al., 2007; Ohshiro et al., 2011, 2017). The divisive normalization operating in these areas is thought to be a canonical feature of multisensory integration, which can account for the way neuronal responses depend on the efficacy and spatial relationship of the individual stimuli (Ohshiro et al., 2011). Our results suggest that this may be a more widespread property of multisensory neurons, even occurring in a structure (i.e. the auditory thalamus) that lacks recurrent connectivity (Bartlett and Smith, 1999).

In contrast to the exclusively suppressive effects of somatosensory stimulation on the MGBv and MGBd, neurons in the medial sector of the auditory thalamus (MGBm, PIN and SGN) exhibited a mixture of crossmodal suppression and enhancement and more than a quarter were driven by whisker stimulation. Somatosensory responses have previously been reported in these areas in other species (Bordi and LeDoux, 1994; Wepsic, 1966). The facilitatory effects of whisker deflection were replicated by optogenetic activation of S1 layer 5 neurons, but were preserved when S1 was silenced. This suggests that they reflect a convergence of top-down corticothalamic and bottom-up inputs from spinothalamic, dorsal column and trigeminal pathways (Jones and Burton, 1974; Lund and Webster, 1967b, 1967a). Neurons in these medial thalamic structures primarily target secondary auditory and higher-level association cortical areas, and the minority that innervate A1 terminate in layer 1 and layer 5/6 (Doron and Ledoux, 2000; Huang and Winer, 2000; Vasquez-Lopez et al., 2017). However, the thalamic axon boutons that we imaged in layer 1 showed exclusively crossmodal suppression of sound-evoked activity, suggesting that neurons whose responses are facilitated or driven by somatosensory inputs project elsewhere in the brain. Their targets include the basal ganglia (Moriizumi and Hattori, 1992; Vasquez-Lopez et al., 2017) and amygdala (Barsy et al., 2020; Bordi and LeDoux, 1994; Doron and Ledoux, 2000; Vasquez-Lopez et al., 2017), with the latter projection being a critical part of the circuitry mediating auditory fear conditioning (Barsy et al., 2020; Cruikshank et al., 1992; Weinberger, 2011).

In addition to differences in their efferent targets and in the effects of somatosensory inputs on their responses to sound, the physiological properties of neurons in the MGBm, PIN and SGN are distinct in other ways from those in the MGBv/MGBd (Smith et al., 2006). Indeed, the lack of excitatory connectivity between these neurons (Bartlett and Smith, 1999) makes the auditory thalamus an ideal place to establish functionally distinct pathways that are independently and flexibly modulated by contextual information, including inputs from other senses or motor commands (Lohse et al., 2019).

Corticofugal crossmodal control of the auditory thalamus

There is growing evidence that descending corticofugal pathways contribute to the processing of sensory information, both within and across sensory modalities, and to integrating sensory and motor signals (Allen et al., 2017; Bajo and King, 2013; Guo et al., 2017; Lohse et al., 2019; Mo and Sherman, 2018). We found that activity in S1 can modulate sound-evoked responses throughout the auditory thalamus, and therefore in the auditory cortex, demonstrating the existence of a trans-thalamic pathway for mediating the influence of somatosensory stimuli on auditory cortical processing. Although auditory cortical feedback can inhibit MGB activity via GABAergic neurons in the TRN (Zhang et al., 2008), this pathway does not appear to be involved in the somatosensory suppression of auditory responses. Instead, this depends on a descending projection from S1 to IC shell neurons that inhibit responses in the MGB. Somatosensory dominance over auditory processing in mouse A1 is therefore implemented by a corticocolliculo-thalamocortical circuit. These findings add to the growing evidence that trans-thalamic circuits enable communication between different cortical areas (Sherman and Guillery, 2011), and demonstrate that the midbrain is also part of the circuitry responsible for integrating multisensory signals across the cerebral cortex.

Interactions between somatosensory and auditory inputs occur as early as the cochlear nucleus in the brainstem (Shore and Zhou, 2006). We did not observe any effects of whisker stimulation on the auditory responses of neurons recorded in the CNIC, the primary relay nucleus of the auditory midbrain, suggesting that multisensory suppression in the MGBv is unlikely to be inherited from earlier in the auditory pathway. However, the lateral shell of the IC receives somatosensory inputs from much of the body via projections from the somatosensory cortex and the brainstem (Aitkin et al., 1981; Lesicko et al., 2016). In mice, these inputs target GAD-67-positive modules that are separated by regions receiving auditory inputs (Lesicko et al., 2016). Furthermore, GABAergic neurons throughout the IC project to the MGB (Beebe et al., 2018; Clarke and Lee, 2018; Peruzzi et al., 1997; Winer et al., 1996). Our data therefore bridge these anatomical studies and establish a functional role for such circuits by demonstrating that a relatively small population of S1-recipient neurons in the lateral shell of the IC are responsible for the suppressive effects of whisker stimulation on sound-evoked responses in the auditory thalamus.

Perceptual implications of somatosensory control over auditory processing

Given its key position in the sensory and motor systems of the brain, context-dependent modulation of neuronal activity in the thalamus has wide-ranging consequences for information processing, not only in the cerebral cortex but also in other thalamorecipient brain regions, such as the amygdala and basal ganglia. The presence of region-specific multisensory interactions throughout the auditory

thalamus therefore implies that combining information from different sensory modalities at this relatively early stage in the processing hierarchy plays a fundamental role in how animals perceive and interact with their sensory environments.

In rats, facial touch is associated with inhibition of the auditory cortex (Rao et al., 2014), potentially reflecting a greater salience of haptic information during social interactions and exploration. Our data suggest that these effects are likely to be present in the thalamus too and that they are asymmetric since we did not observe a comparable modulatory influence of sound on neuronal responses to whisker stimulation in the somatosensory thalamus or cortex (Figure S8). The suppressive effects of somatosensory stimulation on sound-evoked responses, which have now been reported at multiple stages of the auditory pathway, may also help to reduce the impact of vocalizations or other self-generated and potentially distracting sounds, such as those resulting from chewing or breathing (Shore and Zhou, 2006).

Although somatosensory suppression of auditory thalamocortical activity may reflect the relative importance of these inputs when nearby objects are encountered during exploration of the environment, a reduction in the firing rate of auditory neurons in the presence of other sensory cues can be accompanied by an increase in response reliability and in the amount of stimulus-related information transmitted (Bizley et al., 2007; Kayser et al., 2010). Furthermore, auditory cortical activity is suppressed when an animal engages in a task (Otazu et al., 2009). Of particular relevance to the present study is the finding that divisive scaling of auditory cortical frequency tuning, as demonstrated in our recordings, is associated with improved frequency discrimination at the expense of impaired tone detection (Guo et al., 2017). By inducing divisive gain in the auditory thalamocortical system, somatosensory inputs might function as a bottom up cue that sharpens auditory acuity, whilst reducing sensitivity.

Data availability

All relevant data are available on request to, and will be fulfilled by, the lead contact (michael.lohse@dpag.ox.ac.uk).

Code availability

Matlab code for analyses are available on request to, and will be fulfilled by, the lead contact (michael.lohse@dpag.ox.ac.uk).

Methods

Mice

All experiments were approved by the Committee on Animal Care and Ethical Review at the University of Oxford and were licensed by the UK Home Office (Animal Scientific Procedures Act, 1986, amended in 2012). Four strains of male and female mice were used: *C57BL6/J* (Envigo, UK), *VGAT-ChR2-YFP* (JAX 014548 - Jackson Laboratories, USA), *VGAT-cre* (JAX 016962 - Jackson Laboratories, USA), and *C57BL6/NTac.Cdh23*. *C57BL6/J*. *C57BL6/J, VGAT-ChR2-YFP*, and *VGAT-cre* mice were 7–12 weeks old, and *C57BL6/NTac.Cdh23* mice(Mianné et al., 2016) were 10–20 weeks old at the time of data collection. All experiments were carried out in a sound-attenuated chamber.

Stimuli

Auditory stimuli were programmed and controlled in custom-written Matlab code (https://github.com/beniamino38/benware) and generated via TDT RX6 (electrophysiology) or RZ6 (2-photon imaging) microprocessors. Sounds were generated at a ~200 kHz sampling rate, amplified by a TDT SA1 stereo amplifier and delivered via a modified (i.e. sound was 'funnelled' into an otoscope speculum) Avisoft ultrasonic electrostatic loudspeaker (Vifa - electrophysiology) or a TDT EC1 electrostatic speaker (imaging) positioned ~1 mm from the entrance to the ear canal. The sound presentation system was calibrated to a flat (±1 dB) frequency-level response between 1 and 64 kHz. Stimuli included pure tones, covering a frequency range from 2 to 64 kHz, and broadband noise bursts (1-64 kHz). All sounds included 5-ms linear amplitude onset/offset ramps, and unless specified otherwise were presented at 80 dB SPL.

Whisker deflections were delivered with a piezoelectric bimorph attached to a small glass tube. During stimulation, most whiskers were positioned inside the stimulation tube and deflected in a single cosine wave (valley-to-valley), transiently displacing the whiskers 1 mm from resting position at a speed of 40 mm/s.

Presentation of acoustic and whisker stimuli was randomly interleaved, with each sensory stimulus having a duration of 50 ms, unless otherwise specified.

Extracellular recordings

We carried out extracellular recordings using 32- or 64-channel silicon probes (NeuroNexus Technologies Inc.) in a 4 × 8, 8 × 8 or 2 × 32 electrode configuration. Prior to insertion, probes were coated with DiI (Sigma-Aldrich) for subsequent histological verification of the recording sites. Data were acquired using a RZ2 BioAmp processor (TDT) and custom-written Matlab code (https://github.com/beniamino38/benware). Mice were anesthetized with an intraperitoneal

injection of ketamine (100 mg kg^{-1}) and medetomidine (0.14 mg kg^{-1}). Intraperitoneal injections of atropine (Atrocare, 1 mg kg^{-1}) to prevent bradycardia and reduce bronchial secretions and dexamethasone (Dexadreson, 4 mg kg−1) to prevent brain edema were administered. Prior to the surgery, the analgesic bupivacaine was injected under the scalp. The depth of anesthesia was monitored via the pedal reflex and adjusted via small additional doses of the ketamine/medetomidine mix (1/5th of the initial dose) given subcutaneously approximately every 15 min once the recordings had started (~1–1.5 h post induction of anesthesia).

All recordings were performed in the right hemisphere. A silver reference wire was positioned in the visual cortex of the contralateral hemisphere, and a grounding wire was attached under the skin on the neck musculature. The head was fixed in position with a metal bar attached with bone cement to the skull over the left hemisphere. Circular craniotomies (2 mm diameter) were performed above the IC (centered ~5 mm posterior from bregma and ~1 mm lateral from midline), over the visual cortex for auditory thalamic recordings (centered ~3 mm caudal from bregma and ~2.1 mm lateral from midline), and/or over A1 (centered ~2.5 mm posterior from bregma and ~4.5 mm lateral from midline). The exposed dura mater was kept moist with saline throughout the experiment.

Recording sites were considered to be in the CNIC when the units recorded on those sites were part of a clear dorso-ventral tonotopic gradient(Portfors et al., 2011; Stiebler and Ehret, 1985) and the probe's location could be confirmed by post-mortem brain histology. For recordings in the MGB, probe sites were attributed to specific auditory thalamic subdivisions by histological reconstruction of the recording sites (Supplementary Figure 2). We parcellated the auditory thalamus based on previous immunohistochemical descriptions (Lu et al., 2009) and our own pilot tracing experiments from several cortical areas. Accordingly, recording sites were assigned to the ventral division (MGBv), dorsal division (MGBd), medial division and posterior intralaminar nucleus (MGBm/PIN), or suprageniculate nucleus (SGN). Based on these histological reconstructions, recording sites attributed to the MGBv were located <500 µm from the lateral border of the MGB and <500 µm from the deepest acoustically-responsive site, while those in the MGBd were <500 µm from the lateral border of the MGB, but >500 µm from the most ventral acoustically-responsive site. For recordings in the medial sector of the auditory thalamus, sites assigned to the MGBm/PIN were >500 µm from the lateral border of the MGB and <500 µm from the most ventral acoustically-responsive site, and those in the SGN were >500 µm from the lateral border of the MGB and >500 µm from the most ventral acoustically-responsive site.

A1 was identified by robust neuronal responses to broadband noise bursts, and a well-defined caudo-rostral tonotopic axis (Guo et al., 2012; Vasquez-Lopez et al., 2017). Cortical tonotopy was

assessed in all cortical recordings by estimating frequency response areas from responses to pure tones using probes with four recording shanks spaced 200 µm apart and oriented parallel to the caudo-rostral axis.

Two-photon calcium imaging of thalamocortical boutons

We made injections of ~140 nl (diluted 1:1 in PBS) of AAV1.Syn.GCaMP6m.WPRE.SV40 into the auditory thalamus (3 mm caudal from bregma, 2.1 mm lateral from midline and 2.8 - 3 mm ventral from the cortical surface) for expression of GCaMP6m in auditory thalamic neurons and axons as reported previously(Vasquez-Lopez et al., 2017). Mice were administered buprenorphine (Vetergesic 1 ml/kg), dexamethasone (Dexadreson 4 µg), and atropine (Atrocare 1 µg) intraperitoneally and anesthetized with 1.5% isoflurane throughout the surgical procedure. An additional dose of buprenorphine was given 24 hours post-operatively.

In order to visualize the calcium activity of thalamic boutons in layer 1 (20-80 µm below the surface) of the auditory cortex, mice were chronically implanted with a head bar and a circular 4 mm diameter glass window. The implant surgery procedure took place 2-3 weeks following injection of the viral construct. Data acquisition began ~7 days after the implant surgery. Calcium imaging was carried out using a 2-photon laser scanning microscope (B-Scope, Thorlabs, USA). Excitation light of 930 nm (10-50 mW power measured under the objective) was provided by a Mai-Tai eHP (Spectra-Physics, USA) laser fitted with a DeepSee prechirp unit (70 fs pulse width, 80 MHz repetition rate). The laser beam was directed through a Conoptics (CT, USA) modulator and scanned onto the brain with an 8 kHz resonant scanner (x-axis) and a galvanometric scan mirror (y-axis), allowing acquisition of 512x512 pixel frames at ~30 Hz. Emitted photons were guided through a 525/50 filter onto GaAsP photomultipliers (Hamamatsu, Japan). We used ScanImage (Pologruto et al., 2003) to control the microscope during data acquisition and a 16X immersion objective (Nikon, Japan). Mice were kept anesthetized with a mixture of ketamine and medetomidine throughout the experiment (similar to the experiments described in the previous section).

Viral injections and transgenic expression of proteins for optogenetic control

All injections were performed using a custom-made pressure injection system with a calibrated glass pipette positioned in the right hemisphere. The tip of the pipette was carefully and slowly inserted into the area of interest, and ~20 nl boluses were then given every two minutes until the desired volume had been injected. The pipette was then left in position for an additional 5 minutes before being slowly retracted. All optogenetic experiments involving viral injections were carried out >3 weeks after the injection to allow for expression of the opsin. All optogenetic stimulation experiments were carried out with a bright white LED shining into the eyes of the mouse throughout the

545 experiment, to saturate photoreceptor responses in the retina and prevent visual activity being
546 induced by the light stimulation (Danskin et al., 2015).

547 *Activating infragranular cells in S1 using ChrimsonR whilst imaging auditory thalamocortical*
548 *axons and boutons*

549 We injected 120 nL of AAV1-CAG-ChrimsonR (Klapoetke et al., 2014) in S1 (-0.8 and -1.0 mm caudal
550 from bregma, 2.6 mm lateral from midline, and 0.8, 0.65, and 0.5 mm ventral from the cortical surface)
551 to induce expression in the infragranular layers of S1 of C57BL6/J mice. In the same surgery, we also
552 injected AAV1-hSyn-GCaMP6m into auditory thalamus and implanted a glass window over the
553 auditory cortex and a head bar, as explained in the previous section. Finally, in the same surgery, we
554 placed a 400 µm fibre optic cannula on the dura of S1. For optogenetic activation, a 5-7 mW/mm^2, 595
555 nm LED pulse (Doric Lenses, Canada) was delivered to S1 concurrently with, and for the duration of,
556 broadband noise stimulation (i.e. 50 ms or 200 ms).

557 *Activating RBP4+ cells in layer 5 of S1 using ChR2*

558 We injected 60-80 nl of AAV5-DIO-hChR2-eYFP(Nagel et al., 2003) in S1 (0.8 mm caudal from bregma,
559 2.6 mm lateral from midline, and 1.0 mm, and 0.95 and 0.9 mm ventral from the cortical surface) of
560 RBP4-cre mice to induce expression of ChR2 in layer 5 neurons. For optogenetic activation, a 5-7
561 mW/mm^2, 465 nm LED pulse (Doric Lenses) was presented. Light was delivered through a 1 mm fibre
562 acutely positioned on the dura mater above S1 and concurrently with, and for the duration of, sound
563 stimulation (i.e. 50 ms).

564 *Suppressing neuronal activity in the auditory sector of thalamic reticular nucleus using Jaws*

565 In order to transfect cells in the auditory sector of TRN (audTRN) with Jaws, we exploited the fact that
566 the MGB in rodents contains very few inhibitory cells(Winer and Larue, 1996). An injection of 140 nL
567 of the cre-dependent retrograde construct pAAV-CAG-FLEX-rc[Jaws-KGC-GFP-ER2] (Chuong et al.,
568 2014; Tervo et al., 2016) into the MGB (3.0 mm caudal from bregma, 2.1 mm lateral from midline, 2.8-
569 3.0 mm ventral from the cortical surface) of VGAT-cre mice did not label cells inside the MGB, but
570 instead induced Jaws expression in cre-expressing TRN cells that project to the auditory thalamus.
571 After the injection, we placed a 400 µm fibre optic cannula immediately above audTRN. To maximize
572 the light transmission to the transfected area of audTRN the fibre optic cannula was implanted at a
573 22.5° angle (relative to the coronal axis). The anatomical position was histologically confirmed after
574 the end of the experiments. For optogenetic suppression, we used a 120 mW/mm^2, 640 nm laser pulse
575 (Toptica Photonics, Germany) of 150 ms length, which started 25 ms before sound onset.

Intersectional targeting and activation of S1-recipient neurons in the shell of the IC

We induced expression of cre in neurons receiving projections from S1, by injecting 200 nL of AA1-hSyn-cre into S1 (-0.8 and -1.0 mm caudal from bregma, 2.6 mm lateral from midline, and 0.9, 0.7, and 0.5 mm ventral from the cortical surface). This virus anterogradely and transsynaptically infected neurons receiving projections from S1 and induced expression of cre in those neurons (Zingg et al., 2017). In order to target expression of ChR2-YFP to IC neurons that receive input from S1, we also injected 200 nL of the cre-dependent construct AAV5-DIO-ChR2-YFP into the lateral part of the IC. For optogenetic activation, a 10 mW/mm^2, 465 nm LED pulse (Doric Lenses) was delivered through a 1 mm optic fiber acutely positioned on the dura mater above the lateral part of the dorsal IC. Stimulation occurred concurrently with, and for the duration of, sound stimulation (i.e. 50 ms).

Suppressing excitatory neurons in S1 using pan-neuronal expression of Jaws

To determine whether S1 is required for whisker-induced suppression of auditory thalamic responses, we injected 380 nL of AAV8-hSyn-Jaws(Chuong et al., 2014) into S1 (-0.8 and -1.0 mm caudal from bregma, 2.6 mm lateral from midline, and 0.9, 0.7, and 0.5 mm ventral from the cortical surface) of mice genetically corrected for age-related hearing loss (C57BL6/NTac.Cdh23 (Mianné et al., 2016)). For optogenetic suppression of S1 activity during extracellular recordings in the auditory thalamus, a 5-7 mW/mm^2, 635 nm LED pulse (Doric Lenses) was delivered through an acutely positioned 1 mm optic fibre optic placed on the dura mater above S1. Light stimulation started 10 ms prior to the onset of sound stimulation and lasted 250 ms.

Silencing excitatory cortical activity in VGAT-ChR2-YFP mice

For optogenetic silencing of A1 and S1, we used a blue (465 nm) LED stimulus (duration 150 ms, onset 25 ms before auditory and/or somatosensory stimulation) delivered via a 200 µm optic fibre (Doric Lenses) acutely implanted over the dura mater above A1 or the S1 barrel field, respectively. ChR2 was targeted to inhibitory neurons using VGAT-ChR2-YFP mice. Light power was ~15 mW/mm^2.

Histology

For post-mortem verification of the electrophysiological recording sites, viral expression pattern, and anatomical tracing, mice were overdosed with pentobarbital (100 mg/Kg body weight, i.p.; pentobarbitone sodium; Merial Animal Health Ltd, Harlow, UK) and perfused transcardially, first with 0.1 M phosphate-buffered saline (PBS, pH 7.4) and then with fresh 4% paraformaldehyde (PFA, weight/volume) in PBS. Mice used in anatomical experiments were euthanized and perfused >4 weeks after the virus injections. Mice used for acute electrophysiology were perfused as soon as the recordings were finished, while those used for chronic 2-photon imaging were perfused when all imaging sessions were completed. Following perfusion, brains were kept in 4% PFA (weight/volume)

in PBS for ~24 hours. The relevant parts of the brains were then sectioned using a vibratome in the coronal plane at a thickness of 50 or 100 µm. Sections were then mounted on glass slides and covered in a mounting medium with DAPI (Vectashield, Vector Laboratories). Images were acquired with an Olympus FV1000 confocal laser scanning biological microscope. Confocal images were captured using similar parameters of laser power, gain, pinhole and wavelengths with two channels assigned as the emission color; z-stacks were taken individually for each channel and then collapsed. Images were processed offline using Imaris (Zurich, Switzerland) and ImageJ (NIH, MD, USA).

Data analysis and statistics

We clustered potential neuronal spikes using KiloSort(Pachitariu et al., 2016) (https://github.com/cortex-lab/KiloSort). Following this automatic clustering step, we manually inspected the clusters in Phy (https://github.com/kwikteam/phy) and removed noise (movement artefacts, optogenetic light artefacts etc). We assessed clusters according to suggested guidelines published by Stephen Lenzi and Nick Steinmetz (https://phy-contrib.readthedocs.io/en/latest/template-gui/#user-guide). Each cluster (following merging and noise removal) was assigned as either noise (clearly not neuronal spike shape), multi-unit (neuronal and mostly consistent spike shape with no absolute refractory period), or single unit (consistent spike shape with absolute refractory period). All analyses performed on the electrophysiological data were run on a combination of small multi-unit clusters and single units (no differences were found between them). Stimulus-evoked responses were measured as the mean firing rate (spikes/second, sp/s) for the duration of the stimulus presentation. Baseline activity was measured from the mean firing rate of the 90 ms preceding stimulus onset.

For 2-photon imaging of thalamocortical axons and boutons, we carried out standard preprocessing (e.g. registration of image stacks, region of interest selection, trace extraction) of the calcium data, as described in detail elsewhere(Barnstedt et al., 2015; Vasquez-Lopez et al., 2017). Given the slower dynamics of GCaMP6m used to monitor bouton activity from auditory thalamocortical axons, we measured the calcium transient response to a 50 ms stimulus as the mean $\Delta F/F$ over the 16 frames following stimulus onset (i.e. for ~550 ms). Baseline activity was measured as the mean $\Delta F/F$ over the 16 frames preceding stimulus onset.

For estimation of somatosensory modulation of noise responses, we only included units/boutons that showed a statistically significant response during sensory stimulation compared to baseline (*t*-test, $p < 0.005$). For estimation of somatosensory modulation of tone responses, we only

included units/boutons that showed a statistically significant difference in response among the frequency-level combinations tested (one-way ANOVA, $p < 0.005$).

The best frequency (BF) of tone-responsive neurons and boutons was defined as the sound frequency associated with the largest response (i.e. firing rate or $\Delta F/F$, respectively) at the sound level used. For summary statistics and display of summary frequency tuning curves across units/boutons, we normalized the tuning curves of each unit/bouton. To do this, we first estimated the mean frequency tuning curve across conditions (e.g. with and without whisker deflection and/or S1/A1 manipulations), and centered the frequency tuning curves for each condition on the BF estimated from the mean frequency tuning curve. We then normalized the response to each tone frequency presented - separately for each condition - by dividing by the response at the BF in the control condition (i.e. tones presented alone). We then produced a summary frequency tuning curve by taking the median of the normalized frequency tuning curves across units/boutons. Error bars for the summary tuning curves were estimated from bootstrapped (10,000 iterations) 95% nonparametric confidence intervals.

For group (i.e. across units or boutons) comparisons, we used non-parametric statistical tests (i.e. Wilcoxon signed rank for paired samples and Mann–Whitney *U* test for independent samples).

References

Aitkin, L.M., Kenyon, C.E., and Philpott, P. (1981). The representation of the auditory and somatosensory systems in the external nucleus of the cat inferior colliculus. J. Comp. Neurol. *196*, 25–40.

Allen, A.E., Procyk, C.A., Brown, T.M., and Lucas, R.J. (2017). Convergence of visual and whisker responses in the primary somatosensory thalamus (ventral posterior medial region) of the mouse. J. Physiol. *595*, 865–881.

Anderson, L.A., and Linden, J.F. (2011). Physiological differences between histologically defined subdivisions in the mouse auditory thalamus. Hear. Res. *274*, 48–60.

Atilgan, H., Town, S.M., Wood, K.C., Jones, G.P., Maddox, R.K., Lee, A.K.C., and Bizley, J.K. (2018). Integration of visual information in auditory cortex promotes auditory scene analysis through multisensory binding. Neuron *97*, 640–655.

Avillac, M., Ben Hamed, S., and Duhamel, J.R. (2007). Multisensory integration in the ventral

intraparietal area of the macaque monkey. J. Neurosci. *27*, 1922–1932.

Bajo, V.M., and King, A.J. (2013). Cortical modulation of auditory processing in the midbrain. Front. Neural Circuits *6*, 1–12.

Banks, M.I., Uhlrich, D.J., Smith, P.H., Krause, B.M., and Manning, K.A. (2011). Descending projections from extrastriate visual cortex modulate responses of cells in primary auditory cortex. Cereb. Cortex *21*, 2620–2638.

Barnstedt, O., Keating, P., Weissenberger, Y., King, A.J., and Dahmen, J.C. (2015). Functional microarchitecture of the mouse dorsal inferior colliculus revealed through in vivo two-photon calcium imaging. J. Neurosci. *35*, 10927–10939.

Barsy, B., Kocsis, K., Magyar, A., Babiczky, Á., Szabó, M., Veres, J.M., Hillier, D., Ulbert, I., Yizhar, O., and Mátyás, F. (2020). Associative and plastic thalamic signaling to the lateral amygdala controls fear behavior. Nat. Neurosci. 1–13.

Bartlett, E.L., and Smith, P.H. (1999). Anatomic, intrinsic, and synaptic properties of dorsal and ventral division neurons in rat medial geniculate body. J. Neurophysiol. *81*, 1999–2016.

Beebe, N.L., Mellott, J.G., and Schofield, B.R. (2018). Inhibitory projections from the inferior colliculus to the medial geniculate body originate from four subtypes of GABAergic Cells. ENeuro *5*, 1–13.

Bizley, J.K., Nodal, F.R., Bajo, V.M., Nelken, I., and King, A.J. (2007). Physiological and anatomical evidence for multisensory interactions in auditory cortex. Cereb. Cortex *17*, 2172–2189.

Bordi, F., and LeDoux, J.E. (1994). Response properties of single units in areas of rat auditory thalamus that project to the amygdala - I. Acoustic discharge patterns and frequency receptive fields. Exp. Brain Res. *98*, 261–274.

Budinger, E., Heil, P., Hess, A., and Scheich, H. (2006). Multisensory processing via early cortical stages: Connections of the primary auditory cortical field with other sensory systems. Neuroscience *143*, 1065–1083.

Cappe, C., and Barone, P. (2005). Heteromodal connections supporting multisensory integration at low levels of cortical processing in the monkey. Eur. J. Neurosci. *22*, 2886–2902.

Choi, I., Lee, J.Y., and Lee, S.H. (2018). Bottom-up and top-down modulation of multisensory integration. Curr. Opin. Neurobiol. *52*, 115–122.

Chou, X.L., Fang, Q., Yan, L., Zhong, W., Peng, B., Li, H., Wei, J., Tao, H.W., and Zhang, L.I. (2020).

699 Contextual and cross-modality modulation of auditory cortical processing through pulvinar mediated
700 suppression. Elife *9*, e53157.

701 Chuong, A.S., Miri, M.L., Busskamp, V., Matthews, G.A.C., Acker, L.C., Sørensen, A.T., Young, A.,
702 Klapoetke, N.C., Henninger, M.A., Kodandaramaiah, S.B., et al. (2014). Noninvasive optical inhibition
703 with a red-shifted microbial rhodopsin. Nat. Neurosci. *17*, 1123–1129.

704 Clarke, B.A., and Lee, C.C. (2018). Inhibitory projections in the mouse auditory tectothalamic system.
705 Brain Sci. *8*.

706 Cruikshank, S.J., Edeline, J.M., and Weinberger, N.M. (1992). Stimulation at a site of auditory-
707 somatosensory convergence in the medial geniculate nucleus is an effective unconditioned stimulus
708 for fear conditioning. Behav Neurosci *106*, 471–483.

709 Danskin, B., Denman, D., Valley, M., Ollerenshaw, D., Williams, D., Groblewski, P., Reid, C., Olsen, S.,
710 and Waters, J. (2015). Optogenetics in mice performing a visual discrimination task: Measurement and
711 suppression of retinal activation and the resulting behavioral artifact. PLoS One *10*, 1–13.

712 Diamond, M.E., Von Heimendahl, M., Knutsen, P.M., Kleinfeld, D., and Ahissar, E. (2008). "Where" and
713 "what" in the whisker sensorimotor system. Nat. Rev. Neurosci. *9*, 601–612.

714 Doron, N.N., and Ledoux, J.E. (2000). Cells in the posterior thalamus project to both amygdala and
715 temporal cortex: A quantitative retrograde double-labeling study in the rat. J. Comp. Neurol. *425*, 257–
716 274.

717 Fu, K.G., Johnston, T.A., Shah, A.S., Arnold, L., Smiley, J., Hackett, T.A., Garraghty, P.E., and Schroeder,
718 C.E. (2003). Auditory cortical neurons respond to somatosensory stimulation. J. Neurosci. *23*, 7510–
719 7515.

720 Ghazanfar, A.A., Maier, J.X., Hoffman, K.L., and Logothetis, N.K. (2005). Multisensory integration of
721 dynamic faces and voices in rhesus monkey auditory cortex. J. Neurosci. *25*, 5004–5012.

722 Guo, W., Chambers, A.R., Darrow, K.N., Hancock, K.E., Shinn-Cunningham, B.G., and Polley, D.B.
723 (2012). Robustness of cortical topography across fields, laminae, anesthetic states, and
724 neurophysiological signal types. J. Neurosci. *32*, 9159–9172.

725 Guo, W., Clause, A.R., Barth-Maron, A., and Polley, D.B. (2017). A corticothalamic circuit for dynamic
726 switching between feature detection and discrimination. Neuron *95*, 180–194.

727 Huang, C.L., and Winer, J.A. (2000). Auditory thalamocortical projections in the cat: Laminar and areal

patterns of input. J. Comp. Neurol. *427*, 302–331.

Ibrahim, L.A., Mesik, L., Ji, X. ying, Fang, Q., Li, H. fu, Li, Y. tang, Zingg, B., Zhang, L.I., and Tao, H.W. (2016). Cross-modality sharpening of visual cortical processing through layer-1-mediated inhibition and disinhibition. Neuron *89*, 1031–1045.

Iurilli, G., Ghezzi, D., Olcese, U., Lassi, G., Nazzaro, C., Tonini, R., Tucci, V., Benfenati, F., and Medini, P. (2012). Sound-driven synaptic inhibition in primary visual cortex. Neuron *73*, 814–828.

Jones, E.G., and Burton, H. (1974). Cytoarchitecture and somatic sensory connectivity of thalamic nuclei other than the ventrobasal complex in the cat. J. Comp. Neurol. *154*, 395–432.

Kayser, C., Petkov, C.I., Augath, M., and Logothetis, N.K. (2005). Integration of touch and sound in auditory cortex. Neuron *48*, 373–384.

Kayser, C., Petkov, C.I., and Logothetis, N.K. (2008). Visual modulation of neurons in auditory cortex. Cereb. Cortex *18*, 1560–1574.

Kayser, C., Logothetis, N.K., and Panzeri, S. (2010). Visual enhancement of the information representation in auditory cortex. Curr. Biol. *20*, 19–24.

Khorevin, V.I. (1980). Effect of electrodermal stimulation on single unit responses to acoustic stimulation in the parvocellular part of the medial geniculate body. Neurophysiology *12*, 129–134.

Kimura, A., and Imbe, H. (2018). Robust subthreshold cross-modal modulation of auditory response by cutaneous electrical stimulation in first- and higher-order auditory thalamic nuclei. Neuroscience *372*, 161–180.

Kimura, A., Yokoi, I., Imbe, H., Donishi, T., and Kaneoke, Y. (2012). Auditory thalamic reticular nucleus of the rat: Anatomical nodes for modulation of auditory and cross-modal sensory processing in the loop connectivity between the cortex and thalamus. J. Comp. Neurol. *520*, 1457–1480.

Klapoetke, N.C., Murata, Y., Kim, S.S., Pulver, S.R., Birdsey-Benson, A., Cho, Y.K., Morimoto, T.K., Chuong, A.S., Carpenter, E.J., Tian, Z., et al. (2014). Independent optical excitation of distinct neural populations. Nat. Methods *11*, 338–346.

De La Mothe, L.A., Blumell, S., Kajikawa, Y., and Hackett, T.A. (2006). Thalamic connections of the auditory cortex in marmoset monkeys: Core and medial belt regions. J. Comp. Neurol. *496*, 72–96.

Lakatos, P., Chen, C., Connell, M.N.O., Mills, A., and Schroeder, C.E. (2007). Neuronal oscillations and multisensory interaction in primary auditory cortex. Neuron *53*, 279–292.

757 Lesicko, A.M.H., Hristova, T.S., Maigler, K.C., and Llano, D.A. (2016). Connectional modularity of top-
758 down and bottom-up multimodal inputs to the lateral cortex of the mouse inferior colliculus. J.
759 Neurosci. *36*, 11037–11050.

760 Lohse, M., Bajo, V.M., and King, A.J. (2019). Development, organization and plasticity of auditory
761 circuits: Lessons from a cherished colleague. Eur. J. Neurosci. *49*, 990–1004.

762 Lu, E., Llano, D.A., and Sherman, S.M. (2009). Different distributions of calbindin and calretinin
763 immunostaining across the medial and dorsal divisions of the mouse medial geniculate body. Hear.
764 Res. *257*, 16–23.

765 Lund, R.D., and Webster, K.E. (1967a). Thalamic afferents from the spinal cord and the trigeminal
766 nucleus. An experiment anatomic study in the rat. J. Comp. Neurol. *130*, 313–328.

767 Lund, R.D., and Webster, K.E. (1967b). Thalamic afferents from the dorsal column nuclei. An
768 experimental anatomical study in the rat. J. Comp. Neurol. *130*, 301–311.

769 Meredith, M.A., and Allman, B.L. (2015). Single-unit analysis of somatosensory processing in the core
770 auditory cortex of hearing ferrets. Eur. J. Neurosci. *41*, 686–698.

771 Mianné, J., Chessum, L., Kumar, S., Aguilar, C., Codner, G., Hutchison, M., Parker, A., Mallon, A.M.,
772 Wells, S., Simon, M.M., et al. (2016). Correction of the auditory phenotype in C57BL/6N mice via
773 CRISPR/Cas9-mediated homology directed repair. Genome Med. *8*, 1–12.

774 Mo, C., and Sherman, S.M. (2018). A sensorimotor pathway via higher-order thalamus. J. Neurosci.

775 Moriizumi, T., and Hattori, T. (1992). Ultrastructural morphology of projections from the medial
776 geniculate nucleus and its adjacent region to the basal ganglia. Brain Res. Bull. *29*, 193–198.

777 Murray, M.M., and Wallace, M.T. (2012). The neural bases of multisensory processes (Boca Raton (FL):
778 CRC Press/Taylor & Francis).

779 Nagel, G., Szellas, T., Huhn, W., Kateriya, S., Adeishvili, N., Berthold, P., Ollig, D., Hegemann, P., and
780 Bamberg, E. (2003). Channelrhodopsin-2, a directly light-gated cation-selective membrane channel.
781 Proc. Natl. Acad. Sci. *100*, 13940–13945.

782 Ohshiro, T., Angelaki, D.E., and Deangelis, G.C. (2011). A normalization model of multisensory
783 integration. Nat. Neurosci. *14*, 775–782.

784 Ohshiro, T., Angelaki, D.E., and DeAngelis, G.C. (2017). A neural signature of divisive normalization at
785 the Level of multisensory integration in primate cortex. Neuron *95*, 399–411.

786 Otazu, G.H., Tai, L.H., Yang, Y., and Zador, A.M. (2009). Engaging in an auditory task suppresses
787 responses in auditory cortex. Nat. Neurosci. *12*, 646–654.

788 Pachitariu, M., Steinmetz, N.A., Kadir, S., Carandini, M., and Harris, K.D. (2016). Kilosort: realtime
789 spike-sorting for extracellular electrophysiology with hundreds of channels.
790 http://www.biorxiv.org/content/10.1101/061481v1.

791 Perrodin, C., Kayser, C., Logothetis, N.K., and Petkov, C.I. (2015). Natural asynchronies in audiovisual
792 communication signals regulate neuronal multisensory interactions in voice-sensitive cortex. Proc.
793 Natl. Acad. Sci. U. S. A. *112*, 273–278.

794 Peruzzi, D., Bartlett, E., Smith, P.H., and Oliver, D.L. (1997). A monosynaptic GABAergic input from the
795 inferior colliculus to the medial geniculate body in rat. J. Neurosci. *17*, 3766–3777.

796 Pologruto, T.A., Sabatini, B.L., and Svoboda, K. (2003). ScanImage: Flexible software for operating laser
797 scanning microscopes. Biomed. Eng. Online *2*, 1–9.

798 Portfors, C. V., Mayko, Z.M., Jonson, K., Cha, G.F., and Roberts, P.D. (2011). Spatial organization of
799 receptive fields in the auditory midbrain of awake mouse. Neuroscience *193*, 429–439.

800 Rao, R.P., Mielke, F., Bobrov, E., and Brecht, M. (2014). Vocalization-whisking coordination and
801 multisensory integration of social signals in rat auditory cortex. Elife *3*, e03185.

802 Rockland, K.S., and Ojima, H. (2003). Multisensory convergence in calcarine visual areas in macaque
803 monkey. Int. J. Psychophysiol. *50*, 19–26.

804 Sherman, S.M., and Guillery, R.W. (2011). Distinct functions for direct and transthalamic
805 corticocortical connections. J. Neurophysiol. *106*, 1068–1077.

806 Shore, S.E., and Zhou, J. (2006). Somatosensory influence on the cochlear nucleus and beyond. Hear.
807 Res. *216–217*, 90–99.

808 Smiley, J.F., and Falchier, A. (2009). Multisensory connections of monkey auditory cerebral cortex.
809 Hear. Res. *258*, 37–46.

810 Smith, P.H., Bartlett, E.L., and Kowalkowski, A. (2006). Unique combination of anatomy and physiology
811 in cells of the rat paralaminar thalamic nuclei adjacent to the medial geniculate body. J. Comp. Neurol.
812 *496*, 314–334.

813 Song, Y.-H., Kim, J.-H., Jeong, H., Choi, I., Jeong, D., Kim, K., and Lee, S. (2017). A neural circuit for
814 auditory dominance over visual perception. Neuron *93*, 940–954.

815 Stehberg, J., Stehberg, J., Dang, P.T., and Frostig, R.D. (2014). Unimodal primary sensory cortices are
816 directly connected by long-range horizontal projections in the rat sensory cortex. Front. Neuroanat. *8*,
817 1–19.

818 Stiebler, I., and Ehret, G. (1985). Inferior colliculus of the house mouse. I. A quantitative study of
819 tonotopic organization, frequency representation, and tone-threshold distribution. J. Comp. Neurol.
820 *238*, 65–76.

821 Takesian, A.E., Bogart, L.J., Lichtman, J.W., and Hensch, T.K. (2018). Inhibitory circuit gating of auditory
822 critical-period plasticity. Nat. Neurosci. *21*, 218–227.

823 Tervo, D.G.R., Hwang, B.Y., Viswanathan, S., Gaj, T., Lavzin, M., Ritola, K.D., Lindo, S., Michael, S.,
824 Kuleshova, E., Ojala, D., et al. (2016). A designer AAV variant permits efficient retrograde access to
825 projection neurons. Neuron *92*, 372–382.

826 Vasquez-Lopez, S.A., Weissenberger, Y., Lohse, M., Keating, P., King, A.J., and Dahmen, J.C. (2017).
827 Thalamic input to auditory cortex is locally heterogeneous but globally tonotopic. Elife *6*, e25141.

828 Wang, X., Chou, X., Peng, B., Shen, L., Huang, J.J., Zhang, L.I., and Tao, H.W. (2019). A cross-modality
829 enhancement of defensive flight via parvalbumin neurons in zonal incerta. Elife *8*, e42728.

830 Weinberger, N.M. (2011). The medial geniculate, not the amygdala, as the root of auditory fear
831 conditioning. Hear. Res. *274*, 61–74.

832 Wepsic, J.G. (1966). Multimodal sensory activation of cells in the magnocellular medial geniculate
833 nucleus. Exp. Neurol. *15*, 299–318.

834 Winer, J.A., and Larue, D.T. (1996). Evolution of GABAergic circuitry in the mammalian medial
835 geniculate body. Proc Natl Acad Sci U S A *93*, 3083–3087.

836 Winer, J.A., Mariet, R.L. Saint, Larue, D.T., and Oliver, D.L. (1996). GABAergic feedforward projections
837 from the inferior colliculus to the medial geniculate body. *93*, 8005–8010.

838 Wu, C., Stefanescu, R.A., Martel, D.T., and Shore, S.E. (2015). Listening to another sense:
839 somatosensory integration in the auditory system. Cell Tissue Res. *361*, 233–250.

840 Zhang, M., Kwon, S.E., Ben-Johny, M., O'Connor, D.H., and Issa, J.B. (2020). Spectral hallmark of
841 auditory-tactile interactions in the mouse somatosensory cortex. Commun. Biol. *3*, 1–17.

842 Zhang, Z., Liu, C.H., Yu, Y.Q., Fujimoto, K., Chan, Y.S., and He, J. (2008). Corticofugal projection inhibits
843 the auditory thalamus through the thalamic reticular nucleus. J. Neurophysiol. *99*, 2938–2945.

844 Zingg, B., Hintiryan, H., Gou, L., Song, M.Y., Bay, M., Bienkowski, M.S., Foster, N.N., Yamashita, S.,
845 Bowman, I., Toga, A.W., et al. (2014). Neural networks of the mouse neocortex. Cell *156*, 1096–1111.

846 Zingg, B., Chou, X. lin, Zhang, Z. gang, Mesik, L., Liang, F., Tao, H.W., and Zhang, L.I. (2017). AAV-
847 mediated anterograde transsynaptic tagging: Mapping corticocollicular input-defined neural
848 pathways for defense behaviors. Neuron *93*, 33–47.

849